

Article

Design and Optimization of a Mid-Field Wireless Power Transfer System for Enhanced Energy Transfer Efficiency

Daud Khan, Ashfaq Ahmad  and Dong-you Choi * 

Communication and Wave Propagation Laboratory, Department of Information and Communication Engineering, Chosun University, Gwangju 61452, Republic of Korea; daudkhalil700@gmail.com (D.K.); ashfaquetb11@gmail.com (A.A.)

* Correspondence: dychoi@chosun.ac.kr

Abstract: Mid-field wireless power transfer (WPT) offers a compelling solution for delivering power to miniature implantable medical devices deep within the human body. Despite its potential, the current power delivery levels remain constrained, and the design of a compact source structure to focus the transmitter field on such implants presents significant challenges. In this paper, a novel miniaturized transmitter antenna operating at 1.71 GHz is proposed. Leveraging the antenna proximity-coupled feeding technique, we achieve optimal current distribution for efficient power transfer. Additionally, a receiver integrated within the human body is proposed, comprising a slotted ground and a meandering slotted radiating element. This receiver is excited via a coaxial feedline with a truncated ground. Our findings demonstrate wireless power transfer of -23 dB (0.501%) at a distance of 30 mm between the transmitter and receiver, alongside a peak gain of -20 dB with an impedance bandwidth of 39.61%. These results highlight promising advancements in enhancing energy transfer efficiency for deep-implant applications.

Keywords: mid-field; wireless power transfer (WPT); miniaturized; implantable; biomedical



Citation: Khan, D.; Ahmad, A.; Choi, D.-y. Design and Optimization of a Mid-Field Wireless Power Transfer System for Enhanced Energy Transfer Efficiency. *Symmetry* **2024**, *16*, 753. <https://doi.org/10.3390/sym16060753>

Academic Editors: Vasilis K. Oikonomou, Jamal Zbitou and Aziz Oukaira

Received: 2 May 2024
Revised: 11 June 2024
Accepted: 14 June 2024
Published: 17 June 2024



Copyright: © 2024 by the authors. Licensee MDPI, Basel, Switzerland. This article is an open access article distributed under the terms and conditions of the Creative Commons Attribution (CC BY) license (<https://creativecommons.org/licenses/by/4.0/>).

1. Introduction

The progression of healthcare technology has underscored the necessity for creating efficient and compact wireless implantable medical devices capable of delivering power to deeply situated structures within the human body. The emergence of implantable medical devices (IMDs) has ushered in a new era in medical practices, enhancing the functionality of impaired human organs and improving patient healthcare. These healthcare devices rely on efficient implantable antennas for radio frequency (RF) power reception. Traditionally, batteries with limited lifespans have been utilized for these IMDs [1]. Nevertheless, the replacement of batteries at the end of their lifespan necessitates invasive surgery, which poses risks of pain, shock, and even life-threatening complications for the patient. To safeguard patient safety and circumvent the need for invasive procedures, wireless power transfer (WPT) emerges as an ideal solution [2]. The development of wireless power transfer (WPT) systems for implantable medical devices (IMDs) has garnered considerable attention from the scientific community within the biomedical field [3,4].

The development of implantable antennas presents numerous challenges, encompassing size constraints, biocompatibility, patient safety, and tissue coupling [5]. Generally, wireless power transfer (WPT) techniques adopt two main approaches: near-field inductive transmission and far-field radiative transmission [6]. Inductive transmission involves the use of two resonant coils (primary and secondary) positioned in close proximity to facilitate power transfer to implantable medical devices (IMDs) at low frequencies. Significant research efforts have been directed towards the configuration of near-field WPT systems operating at frequencies such as 0.1–1 MHz [7], 6.78 MHz [8], 13.56 MHz [9], 39.89 MHz [10], 71 MHz [11], 300 and 700 MHz [12], and 500 MHz [13]. Nonetheless, this method frequently demonstrates suboptimal power transfer efficiency (PTE) of $\leq 47\%$, attributable to

its susceptibility to misalignment, small coupling coefficient, and the low quality factor (Q) of the two coils [14].

Furthermore, non-radiative approaches are typically tailored for short-range applications. Moreover, the efficiency of these non-radiative methods heavily depends on the lateral and angular alignment between the transmitting (Tx) and receiving (Rx) sections [15]. The challenges associated with non-radiative wireless power transfer (WPT) systems limit their practical use in powering implantable medical devices (IMDs). This creates an urgent demand for the development of highly efficient WPT systems that can overcome these limitations, ensuring reliable and real-time power delivery to IMDs.

A multitude of investigations have delved into the operation of wireless power transfer (WPT) devices in the far-field region across a range of frequencies, encompassing 2.45 GHz [16], 5.8 GHz [17], and 0.412/0.915/1.2 GHz [18]. Far-field WPT exhibits reduced sensitivity to misalignments between the transmitter (Tx) and the receiver (Rx) across extended distances. However, it suffers from the drawback of a low power transfer efficiency (PTE) of $\leq 1\%$ compared to near-field WPT [19].

Recently, studies have identified an optimal frequency range for wireless power delivery deep into biological tissue, aiming to maximize power transfer efficiency [20,21]. At distances of several centimeters between the Tx and Rx, operating WPT in the low-GHz frequency range corresponds to the mid-field, where the wavelength is comparable to the separation distance. In this mid-field region, the evanescent field transforms into propagating modes upon interaction with biological tissue, facilitating power propagation through multi-layered tissue to the implanted device. By carefully designing the source, significant power delivery can be achieved, mitigating attenuation and dispersion effects within human tissue [22].

Several methods have been suggested to improve the connection between the transmitter (Tx) and receiver (Rx) while also avoiding the need for strict positioning requirements. In [23], the authors introduced the concept of utilizing a parasitic patch to increase the coupling efficiency using a circularly polarized antenna. Additionally, Ref. [24] examines the application of a near-field plate to enhance the coupling efficiency in a radiative wireless power transfer (WPT) system. This is achieved by regulating the power leakage from the transmitter. In [25,26], a high dielectric matching layer, with $\epsilon_r = 78$, was applied on the surface of the skin in an intermediate-range WPT system. This layer decreases the dielectric contrast between air and tissue, consequently enhancing the transmission characteristics. In a recent development highlighted in [27], a metamaterial based on polarization conversion was introduced to enhance the efficiency of wireless power transfer (WPT). Many of these investigations involved transitional elements like metamaterials or matching layers near the skin surface. However, it is important to acknowledge that such setups pose challenges in practical applications due to the complexities involved in implementation.

This study demonstrates an effective mid-field wireless power system for compact implantable medical applications, featuring a miniaturized receiver (Rx) antenna with dimensions of $10 \times 13 \text{ mm}^2$ implanted inside the body, powered by a transmitter (Tx) antenna positioned at a subwavelength distance above the phantom. Both Tx and Rx operate at 1.71 GHz, optimizing the balance between power transfer efficiency and tissue absorption. The Rx antenna exhibits a peak gain of -20 dBi , ensuring effective power reception despite its small size. Compared to traditional methods, our system offers enhanced power transfer efficiency, a more compact and efficient design, optimized frequency selection to mitigate absorption rates, and practical implementation demonstrated in the skin phantoms. These advancements set a new benchmark in the field of wireless power transfer for implantable medical devices. Figure 1 presents the proposed Tx antenna and the implantable antenna within the skin and head phantoms.

The remainder of this paper unfolds in the following manner: Section 1 delves into the introduction and recent trends in the field. In Section 2, the methodology is discussed, focusing on the design aspects of the transmitter (Tx) and receiver (Rx). Section 3 is

dedicated to presenting the results and engaging in a discussion thereof. Finally, Section 4 provides conclusions, summarizing the key findings and implications of the study.

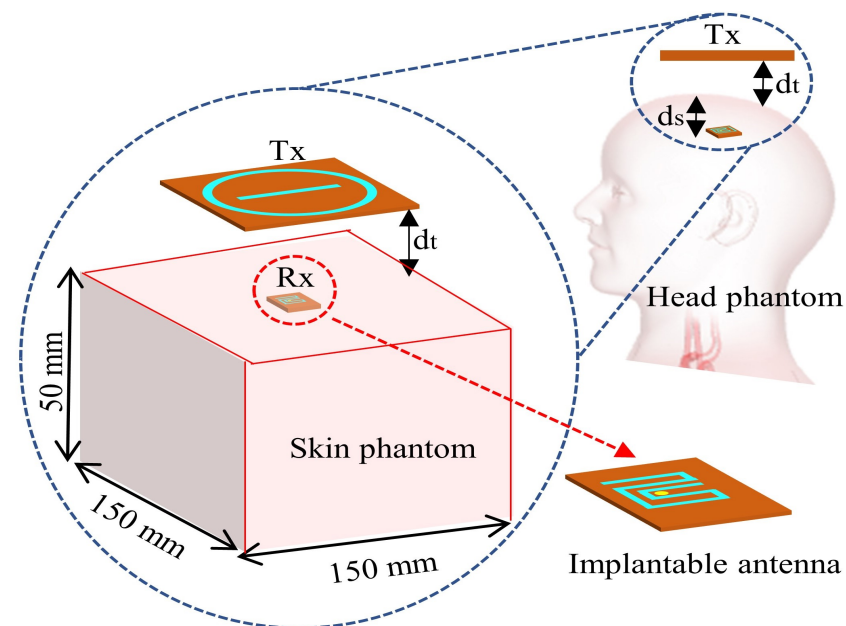


Figure 1. Schematic of the proposed mid-field WPT system.

2. Methods

In this section, the design of the aperture-fed Tx antenna in free space and the Rx antenna in a biomedical environment is presented. The operating frequency of 1.71 GHz was chosen based on a combination of theoretical analysis, simulation studies, and empirical validations. This frequency was selected because it provides an optimal balance between penetration depth and spatial resolution for our specific application and implantation depth. Although ISM frequencies were considered, our analyses demonstrated that 1.71 GHz offers superior performance in terms of efficiency and effectiveness, given the dielectric properties of biological tissues and the specific requirements of our system. Extensive simulations and experimental measurements on tissue phantoms consistently confirmed that 1.71 GHz is within the optimal range, ensuring reliable and reproducible results.

2.1. Implantable Rx Design

In a wireless power transfer system the most crucial part is the Rx implantable antenna because it is situated in the lossy and complex biomedical environment. For the implantable antenna, it is desired to have a compact size, easy configuration, simple structure, good performance, and be bio-compatible with the human body. The front and back views of the proposed implantable antenna are presented in Figure 2a,b, respectively. A meander-line slotted part is the main radiator, while a “C”-shaped slot is made in the ground plane. The antenna is fed using a coaxial feed port with a diameter of 0.4 mm, possessing a characteristic impedance of 50Ω at the impedance-matching point. The antenna’s overall dimensions are $10 \times 13 \times 1.2 \text{ mm}^3$. Roger 6010 is used as a substrate, having a relative permittivity (ϵ_r) of 10.2, tangent loss of 0.002, and a thickness of 1.2 mm.

A meandering antenna is the best candidate and prime choice for an implantable antenna for various reasons. This technique offers numerous benefits, including compactness and space efficiency, an extended operative length, improved impedance matching, and reduced electromagnetic interference [28]. The design, optimization, and miniaturization of the proposed antenna are accomplished through several steps, outlined as steps 1–5 and illustrated in Figure 3. One of the techniques employed involves introducing several slotted meander lines in the radiator to elongate the current path. This method is widely recognized as an effective approach for miniaturizing implantable antennas [29].

The slight capacitive gap between adjacent meander lines is pivotal in augmenting the antenna's impedance-matching traits through mutual impedance. Additionally, the parasitic capacitance between adjacent elements aids in shifting the resonant frequency toward the lower end of the spectrum. In contrast to prior research [24,25,30], this design eliminates the need for vias to minimize size, rendering it economical and simple to produce. Furthermore, employing a slotted ground plane further reduces the antenna's size. The ground slots contribute to efficient performance and excellent impedance matching, as demonstrated in the Section 3.

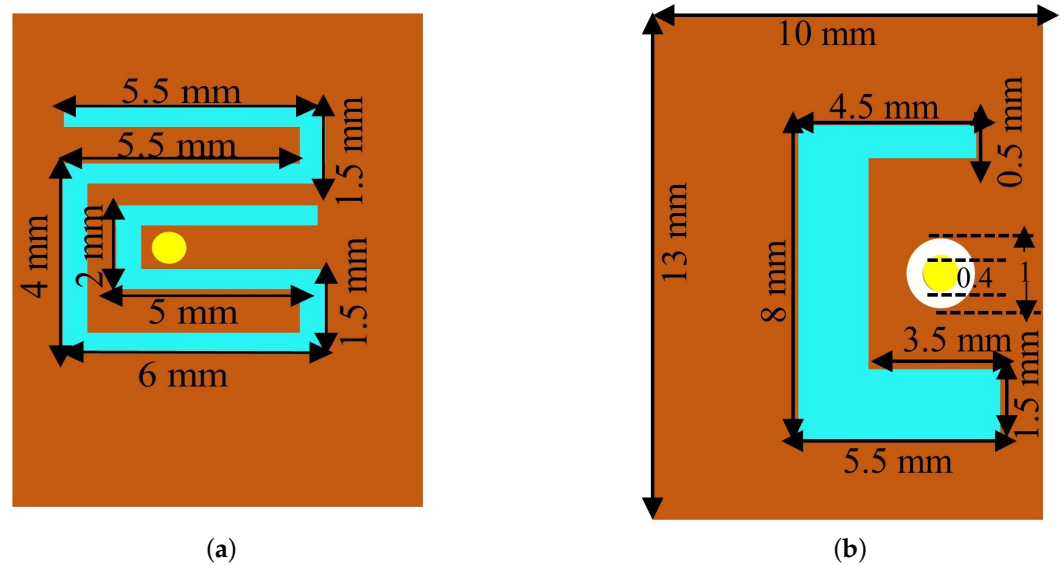


Figure 2. Detailed structure of the implantable antenna: (a) The front view and (b) the back view.

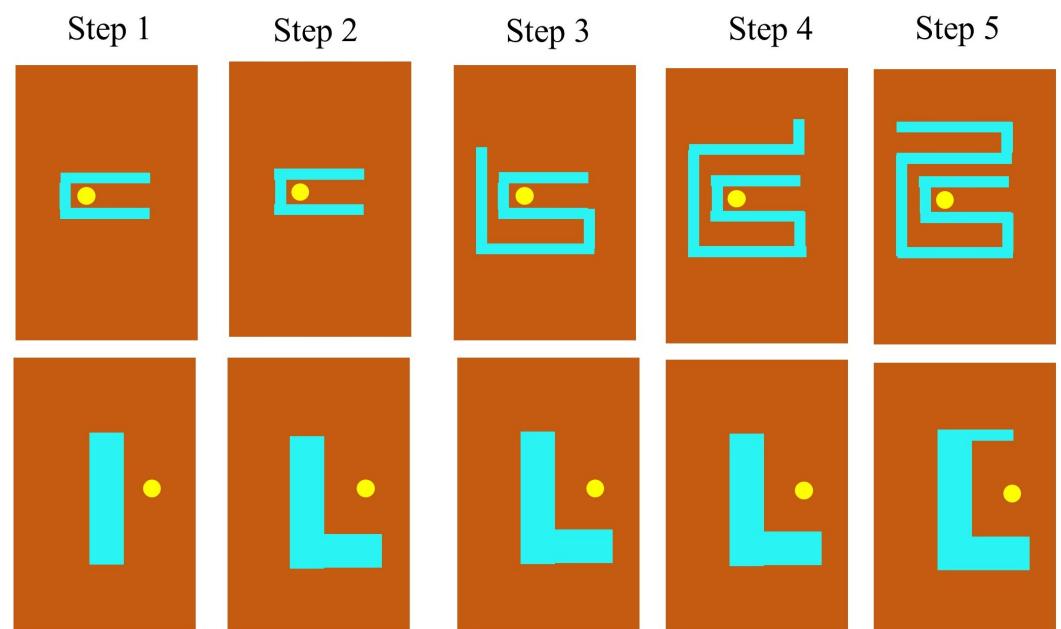


Figure 3. Design and optimization process of the proposed implantable antenna.

2.2. Tx Design

The geometrical configuration of the proposed transmitting antenna is presented in Figure 4. A multi-layered transmitter is designed consisting of two substrates, a radiating part, an aperture, and a feeding line. Taonic TLY-5 is used as a substrate having a relative permittivity (ϵ_r) of 2.2 and a loss tangent of 0.0009. The radiator featuring a circular slot

surrounding an I-shaped slot at its center is designed on the top of substrate “2”, having a thickness of 1.2 mm, while the microstrip feedline is situated at the bottom of substrate “1”, having a thickness of 0.8 mm, which is used to facilitate the dominant magnetic polarization mechanism. Centering the coupling aperture on the ground results in lower cross-polarization due to the configuration’s symmetry [31]. The coupling from the feedline to the source highly depends on the shape and dimensions of the aperture; therefore, it is a prime choice to select a shape of the aperture that maximizes the coupling for a given size. In this study, a circular ring slot printed on the ground, as illustrated in Figure 4c, is proposed. This design offers a smaller size and greater electrical length compared to the traditional shapes. The reduced aperture area contributes to lower back-radiation levels, minimizing spurious radiation and enhancing antenna performance. Additionally, the increased electrical length fosters stronger coupling with the radiating element. The surface current distribution of the circular slotted radiator is illustrated in Figure 5a. It is evident from the figure that the maximum current is concentrated near the circular slot, moving towards the central I-shaped slot, strategically positioned to focus the magnetic field toward the receiver, as illustrated in Figure 5b.

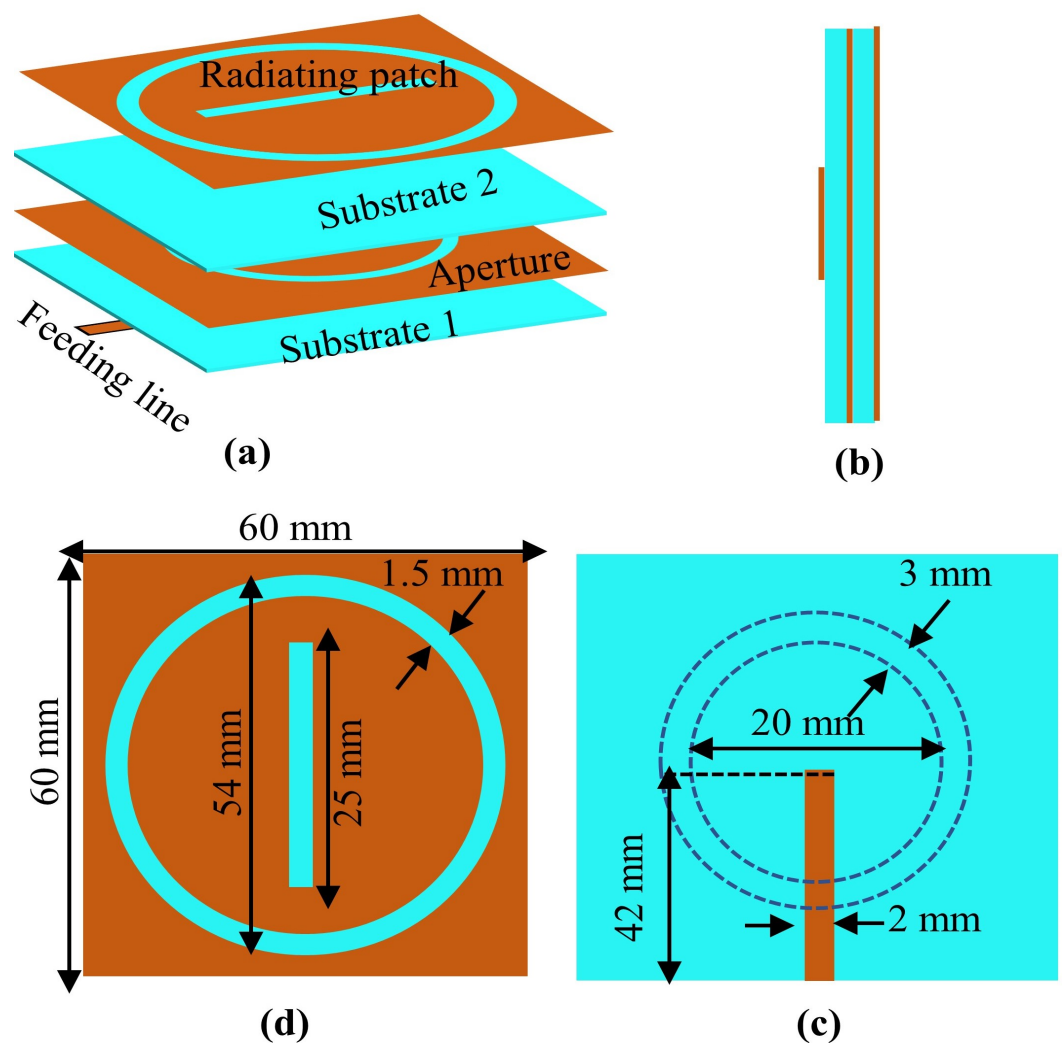


Figure 4. Detailed structure of the transmitting antenna (unit: mm). (a) Isometric view. (b) Side view. (c) Dimensions of the aperture and feedline. (d) Front view.

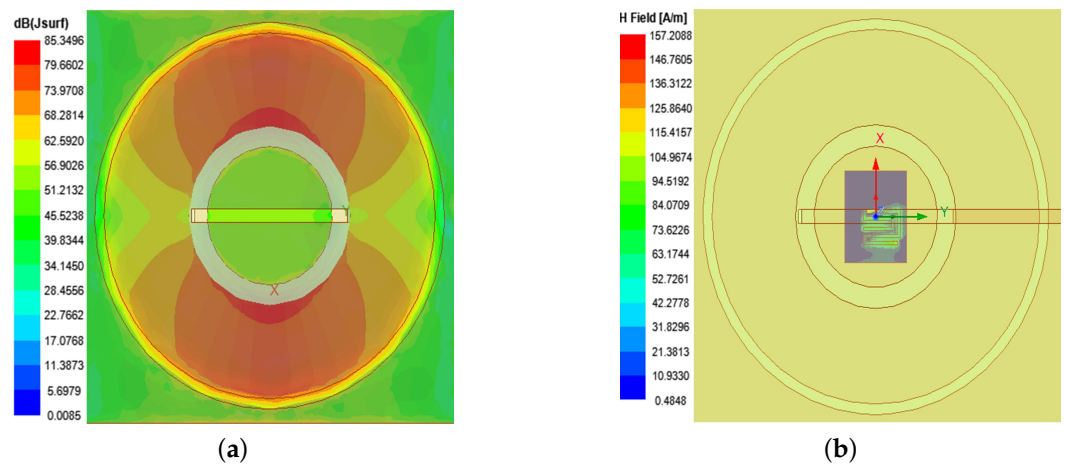


Figure 5. (a) Surface current distribution. (b) Magnetic field distribution.

3. Results and Discussion

The proposed wireless power transfer (WPT) system underwent design and analysis utilizing the HFSS simulation software. Initially, a homogeneous skin phantom (HSP) measuring $150 \times 150 \times 50 \text{ mm}^3$, was used in the WPT system, as depicted in Figure 1. The implantable receiver was positioned at a depth (d_s) of 8 mm within the phantom while maintaining a gap (d_t) of 8 mm between the HSP surface and the external Tx element.

One fundamental aspect to understand about dielectric properties (ϵ_r , σ) is their dependence on the frequency of the electromagnetic waves interacting with the material. As the frequency changes, the response of the material to the electric field also changes [32]. This frequency dependence is often characterized by the material's frequency response, which describes how its dielectric properties vary across different frequencies. This simulation considers skin tissue's dielectric properties, accounting for frequency dependence. A dielectric constant of $\epsilon_r = 41$ and $\sigma = 1.08 \text{ S/m}$ at 1.71 GHz are used in this simulation. Subsequently, employing the finite element method (FEM) within HFSS, the scattering parameters were computed. This encompassed the determination of reflection coefficients (S11, S22) along with transmission coefficients (S21).

Figure 6 illustrates the reflection coefficient (S11) of the receiver (Rx). The analysis indicates that the proposed implantable antenna achieves a reflection coefficient of -32 dB at the resonant frequency of 1.71 GHz. Furthermore, the antenna exhibits a wide operating range, from 1.38 GHz to 2.37 GHz, ensuring versatility in frequency compatibility. Additionally, Figure 7 explores and presents the impact of the slotted meander line and the ground plane configuration on the parameter, demonstrating progressive changes from step 1 to step 5. In the preliminary simulation configuration, the receiving antenna was kept at a depth of $d_s = 8 \text{ mm}$.

Furthermore, real-world scenarios often introduce uncertainties regarding the precise implantation depth due to locational variations. To observe the antenna's robustness across various implantation depths, its effect was observed with d_s varying from 4 to 20 mm, incremented by 4 mm steps. The results demonstrate minimal impact on the antenna's scattering parameters within the desired frequency range, as depicted in Figure 8, highlighting the impressive stability of the proposed implantable antenna. Moreover, the stable performance across various depths suggests the suitability of the proposed antenna for a wide range of implantable applications.

The proposed implantable antenna exhibits a remarkable maximum gain of -20 dB , indicating its efficiency in capturing and utilizing electromagnetic energy.

Figure 9 provides a comprehensive view of the antenna radiation characteristics through its 2D radiation pattern, highlighting both the E and H planes. The radiation pattern demonstrates a distinct directional preference, with the antenna exhibiting its highest gain toward the transmitter (Tx). Although some side and back lobes are present

due to the truncated ground plane, the focused radiation pattern significantly enhances the antenna's power-receiving capabilities, ensuring optimal energy transfer efficiency in the targeted direction. Furthermore, Figure 10 provides detailed insight into the antenna's radiation characteristics through its 3D radiation patterns. These patterns reveal some side and back lobes due to the truncated ground plane, but overall, they highlight the antenna's suitability for implantable applications. This observation reaffirms the antenna's directional efficiency, which is crucial for optimizing power transfer and minimizing spurious radiation in biomedical contexts.

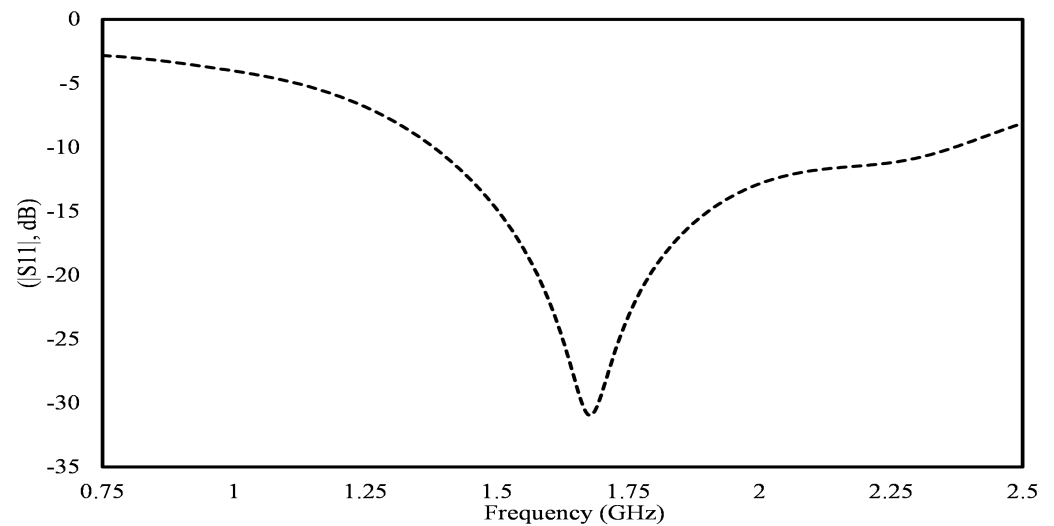


Figure 6. Scattering parameter of the implantable antenna.

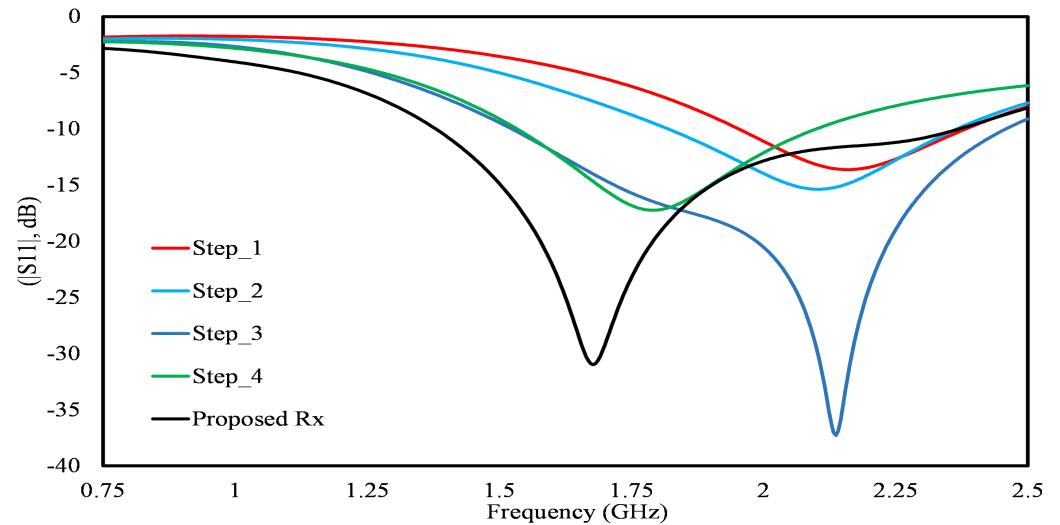


Figure 7. Optimization of the proposed receiving antenna across desired frequency bands: Evaluating the impact of slotted meander lines and ground slots on $|S_{11}|$ at each iterative stage.

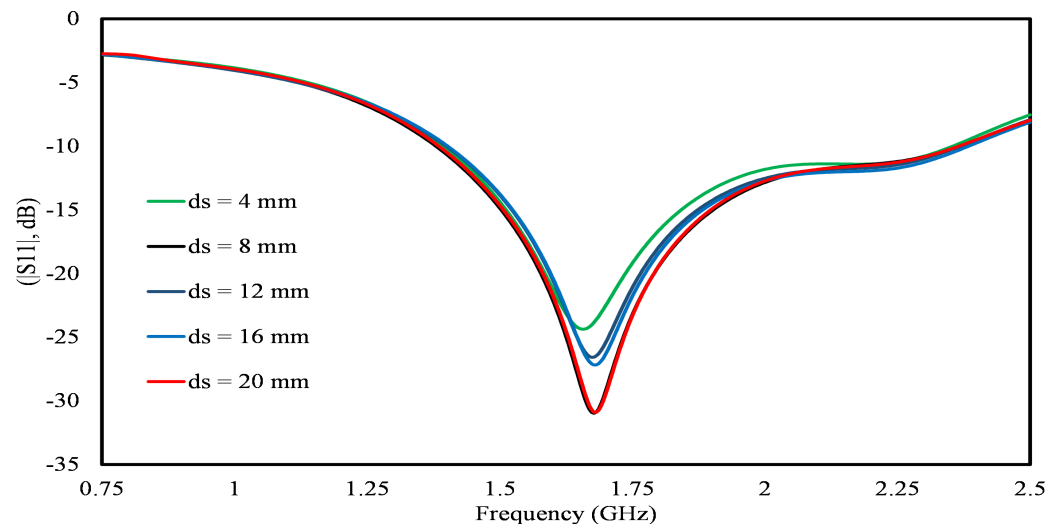


Figure 8. Effects of the depth (d_s) on the scattering parameters of the proposed implantable antenna.

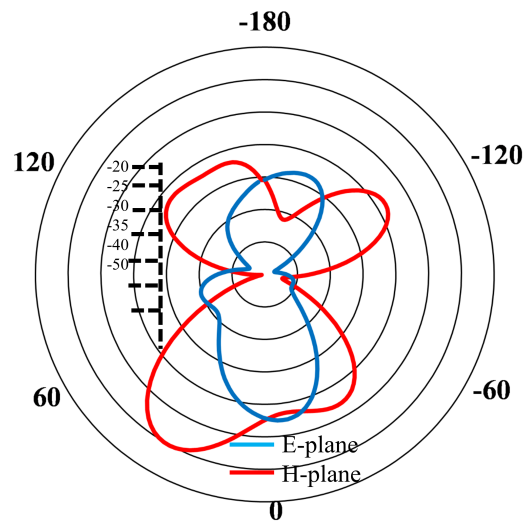


Figure 9. The 2D radiation pattern of the implantable antenna.

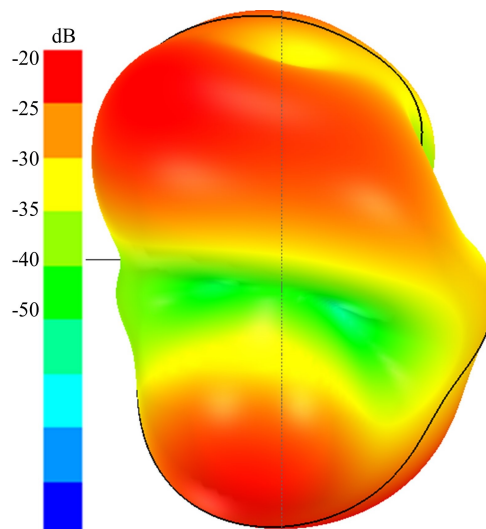


Figure 10. The 3D radiation pattern of the implantable antenna.

In Figure 11, the reflection coefficient (S_{22}) of the transmitting antenna is depicted. The transmitter resonates at 1.71 GHz, exhibiting a -10 dB bandwidth from 1.66 GHz to

1.765 GHz. This bandwidth ensures efficient transmission within the desired frequency range, contributing to the robust performance of the transmitting antenna.

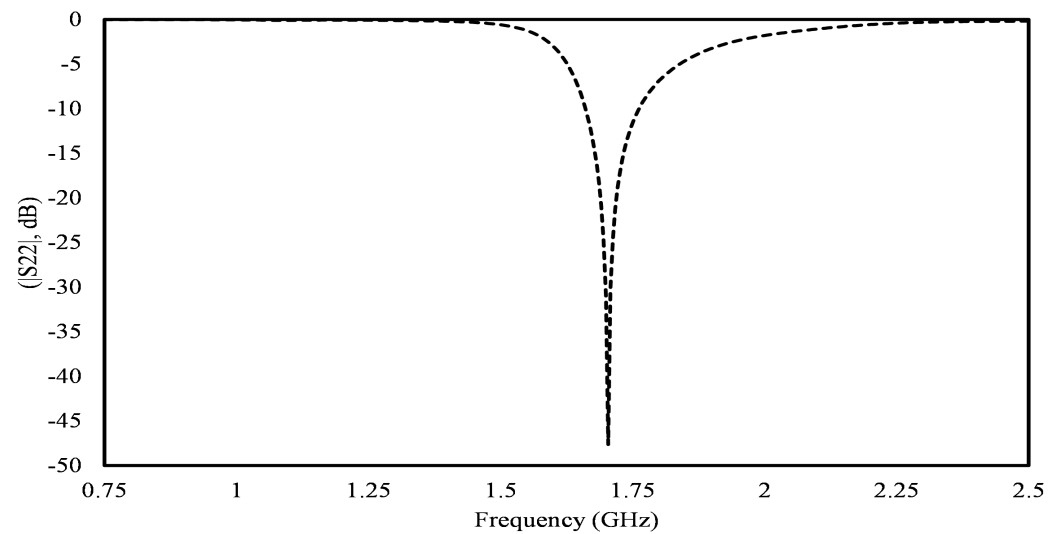


Figure 11. Reflection coefficient (S_{22}) of the Tx antenna.

The transmitting antenna showcases a notable maximum gain of 5.2 dB precisely at the desired frequency. Figure 12 shows the 2D radiation pattern of the proposed antenna, presenting both the E and H planes. It is observed from the figure that the proposed design has minimal back lobes, with maximum power radiating toward the Rx antenna. Figure 13 provides a comprehensive depiction of the antenna's radiation characteristics through a 3D radiation pattern, revealing the distribution of power in three-dimensional space. Notably, the pattern highlights the peak power concentration being directed towards the desired receiver, significantly bolstering the efficiency of power transfer. This directional radiation pattern plays a pivotal role in ensuring optimal energy transmission to the intended recipient, thereby enhancing the overall effectiveness and reliability of the transmitting antenna.

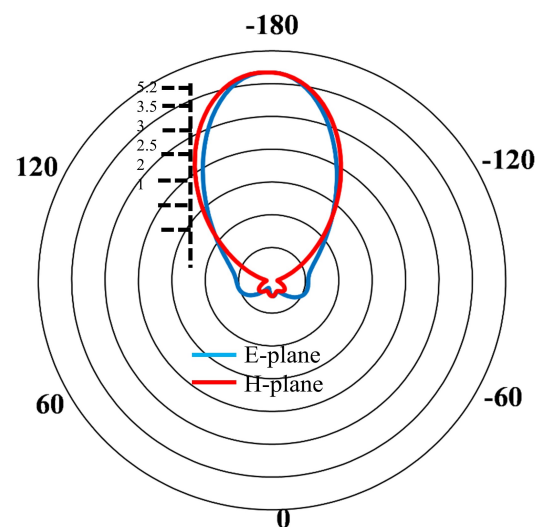


Figure 12. The 2D radiation pattern of the Tx antenna.

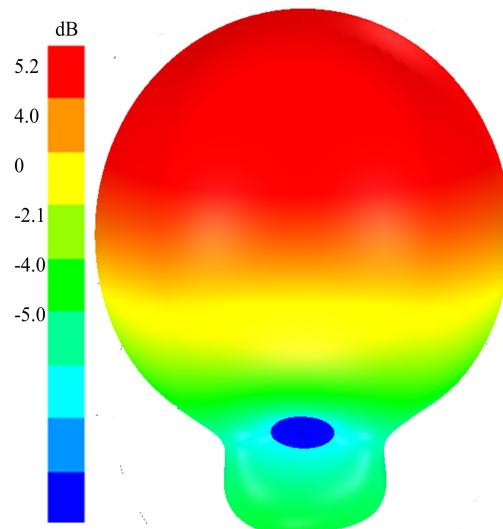


Figure 13. The 3D radiation pattern of the Tx antenna.

The transmission coefficient (S_{21}) serves as a valuable metric for verifying power transfer efficiency. Additionally, the efficiency of power transfer can be quantified using the following equation:

$$\eta = 10 \log(P_2/P_1) \quad (1)$$

where η represents the efficiency in dB, P_2 denotes the received power by the implantable antenna, and P_1 signifies the source power. Careful consideration was given to the orientation of the implantable antenna relative to the mid-field Tx source. The simulation setup positioned the Tx parallel to the skin tissue, maintaining a consistent distance of dt mm above the air–skin tissue interface. The power transfer efficiency (PTE) was observed at different distances (dt) between the transmitter (Tx) and the body surface, ranging from 0 mm to 10 mm. As illustrated in Figure 14, the PTE for distances from 10 mm to 2 mm is close to -23 dB, corresponding to a PTE of approximately 0.501%. The transmitter was positioned 10 mm from the surface of the phantom to balance signal strength and minimize interference. Placing the transmitter directly on the surface could lead to excessive signal attenuation and reflections. The 10 mm distance was chosen based on preliminary simulations, which indicated optimal performance at this spacing. This choice also accounts for practical design constraints, including space for mounting hardware and ensuring consistent signal quality. This visualization enables a comprehensive understanding of how efficiently power is transmitted from the source to the implantable antenna, facilitating the evaluation and optimization of the system's overall functionality and reliability.

In a real-world scenario, it is quite likely that misalignment between the transmitter (Tx) and receiver (Rx) will be encountered, which can compromise the stability of wireless power transmission. To address this, we examine the impact of both lateral and angular misalignments on the S_{21} parameter of the proposed wireless power transfer (WPT) system. Lateral misalignment is analyzed by shifting the Rx horizontally away from the centerline by an offset distance, dy (ranging from 0 to 20 mm), as illustrated in Figure 15a. Angular misalignment, which can occur due to body movements or inaccurate placement of the implantable medical devices (IMDs) after implantation, is studied by rotating the Rx element at varying angles (θ) from 0° to 40° degrees, as shown in Figure 15b. Figure 15a,b demonstrate that the proposed WPT system maintains stability and flexibility despite these misalignments.

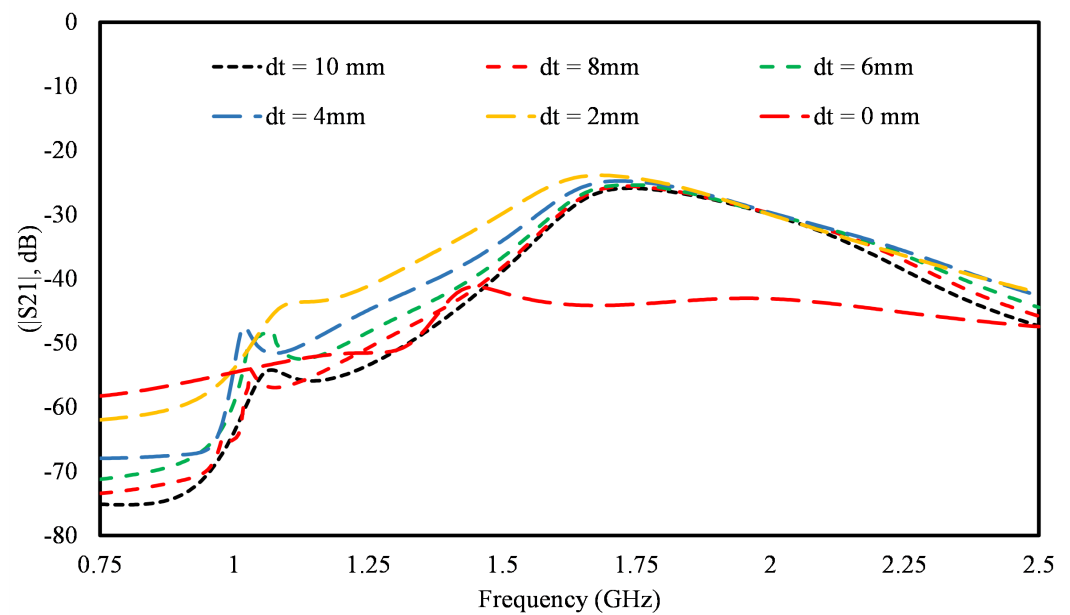


Figure 14. S_{21} of the proposed wireless power system for various dt .

We extended our simulations to include an inhomogeneous medium composed of a model with layers of air, skin, fat, muscle, and heart tissue. The tissue layers and their respective thicknesses were selected to approximate the properties of the human body, specifically 2 mm of skin, 4 mm of fat, 10 mm of muscle, and 15 mm of heart tissue. In our simulations, the transmission coefficient (S_{21}) for the inhomogeneous model was found to be -23 dB, corresponding to a power transfer efficiency (PTE) of approximately 0.501%. In contrast, the homogeneous medium yielded an S_{21} of -25 dB, which equates to a PTE of 0.316%. Figure 16 presents the transmission coefficients for both scenarios, highlighting the differences between homogeneous and inhomogeneous tissue models.

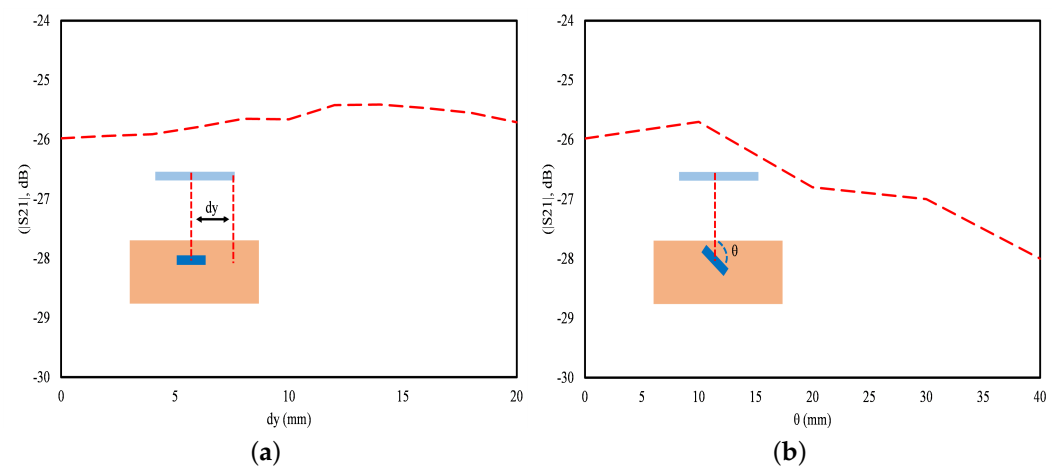


Figure 15. Configuration of S_{21} (dB): (a) lateral and (b) angular misalignment.

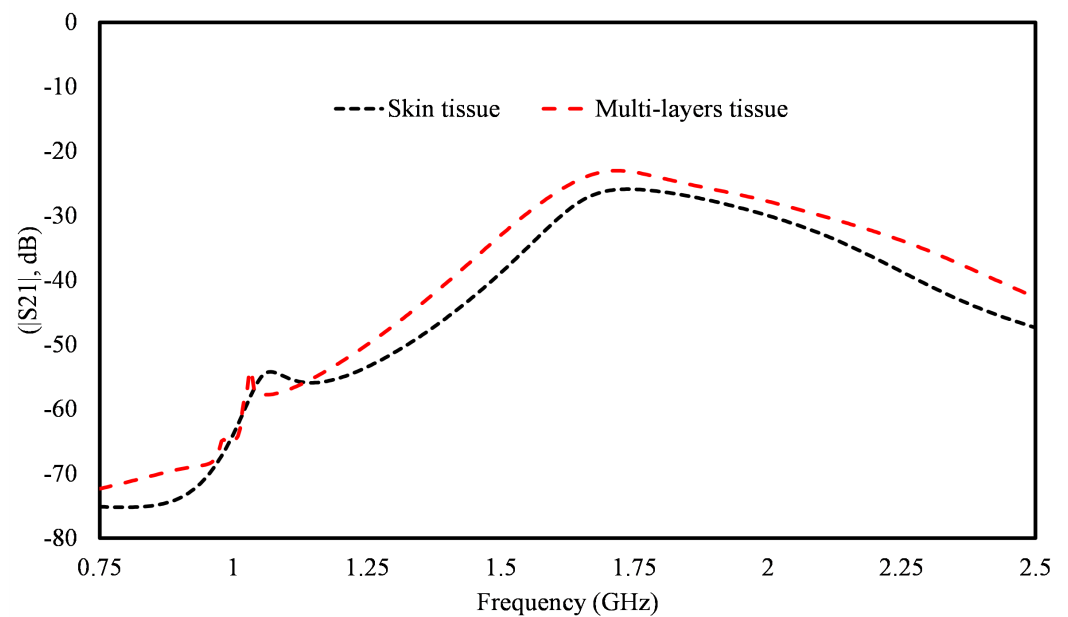


Figure 16. Power transfer efficiency (PTE) for single-layer and multi-layer tissue models.

This work is compared with state-of-the-art designs in the literature as presented in Table 1, the comparisons are made in terms of wireless power transfer technique, transfer distance between the Tx and Rx, and power transfer efficiency (PTE). Additionally, the implantable antenna (Rx) and transmitting antenna (Tx) are compared in terms of gain, bandwidth, reflection coefficient, and dimensions. It is observed from the table that the proposed design demonstrates superior performance in terms of gain, PTE, and bandwidth, highlighting the effectiveness and innovation of our approach. In [33], the system operates at 1.5 GHz with a bandwidth of 0.62 GHz, and the Tx dimensions are $65 \times 65 \text{ mm}^2$. Similarly, in [34], a WPT efficiency of -37 dB is observed compared to -25 dB in the proposed system. A power transfer efficiency of -25 dB is also reported in [30] but with a gain of -26.8 dB . In [16], a far-field wireless power transfer approach is used; however, a PTE of -28.1 dB and a gain of -23 dB are presented.

Table 1. Comparison table.

Comparison Table		[33]	[34]	[30]	[16]	This Work
WPT System	WPT Technique	Mid-Field	Near-Field	Near-Field	Far-Field	Mid-Field
	Transfer Distance	55 mm	60 mm	0.1267λ	150 mm	30 mm
	PTE S21 dB,%	$-22.5 (0.56)$	$-37 (0.0199)$, $-23.7 (0.42)$	$-25 (0.316)$	$-28.1 (0.1549)$	$-23 (0.501)$
Implantable Antenna (Rx)	Dimensions (mm^2)	9×13	5×5.25	5.6×6	5×5	10×13
	Operating Frequency	1.5 GHz	0.915, 2.45 GHz	1900 MHz	2.45 GHz	1.71 GHz
	Bandwidth (GHz)	0.62 GHz	1.45, 0.82 GHz	0.9 MHz	1.2 GHz	0.99 GHz
	S11 (dB)	-30	$-24, -29$	-25	-40	-32
	Gain (dB)	-20	$-22.1, -19.6$	-26.8	-23	-20

Table 1. Cont.

Comparison Table	[33]	[34]	[30]	[16]	This Work	
Transmitting Antenna (Tx)	Dimensions (mm ²)	65 × 65	53 × 83	50 × 50	90 × 130	60 × 60
	Operating Frequency	1.5 GHz	0.915, 2.45 GHz	1900 MHz	2.45 GHz	1.71 GHz
	Bandwidth (GHz)	0.4 GHz	1.9 GHz	0.98 GHz	0.9 GHz	0.105 GHz
	S22 (dB)	−17	−30	−30	−30	−47
	Gain (dB)	-	-	-	8.1	5.2

4. Conclusions

In this paper, a mid-field wireless power transfer system for implantable medical devices (IMDs) is designed. The transmitter proposed uses aperture coupling, while a slotted ground and meandering slotted radiating element is proposed as a receiver. The transmitter exhibits a gain of 5.2 dB, while the receiver, placed inside the phantom, achieves a gain of −20 dB. With the transmitter positioned 10 mm above the skin phantom and the receiver at a depth of 20 mm inside the phantom, the system performance is evaluated at a distance of 30 mm between the transmitter and receiver. The observed power transfer efficiency (PTE) of −23 dB falls within the acceptable range for efficient power delivery. This underscores the suitability of the proposed system for powering IMDs deep within the human body. In conclusion, this study presents a promising solution for wirelessly powering IMDs, offering potential advancements in medical technology. Future research could focus on further optimizing system parameters and exploring real-world implementation scenarios to enhance the practical utility of the proposed system.

Author Contributions: Conceptualization, A.A. and D.K.; data curation, A.A. and D.K.; funding acquisition, D.-y.C.; methodology, A.A. and D.-y.C.; project administration, A.A. and D.-y.C.; resources, A.A. and D.-y.C.; software, A.A. and D.K.; supervision, D.-y.C.; validation, A.A. and D.-y.C.; writing—original draft, D.K. and A.A.; writing—review and editing, A.A. and D.-y.C. All authors have read and agreed to the published version of the manuscript.

Funding: This study was supported by a research fund from Chosun University, 2024.

Data Availability Statement: Data are contained within the article.

Conflicts of Interest: The authors declare no conflicts of interest.

References

- Naser, M.; Al Bazar, H.; Abdel-Jaber, H. Investigational Study for Overcoming Security Challenges in Implantable Medical Devices. *Int. J. Comput. Digit. Syst.* **2024**, *16*, 1–10.
- Mahmud, S.; Nezaratizadeh, A.; Satriya, A.B.; Yoon, Y.K.; Ho, J.S.; Khalifa, A. Harnessing metamaterials for efficient wireless power transfer for implantable medical devices. *Bioelectron. Med.* **2024**, *10*, 7. [[CrossRef](#)] [[PubMed](#)]
- Das, R.; Moradi, F.; Heidari, H. Biointegrated and wirelessly powered implantable brain devices: A review. *IEEE Trans. Biomed. Circuits Syst.* **2020**, *14*, 343–358. [[CrossRef](#)] [[PubMed](#)]
- Ahire, D.; Gond, V.J.; Chopade, J.J. Compensation topologies for wireless power transmission system in medical implant applications: A review. *Biosens. Bioelectron. X* **2022**, *11*, 100180. [[CrossRef](#)]
- Hu, X.Y.; Yin, W.L.; Du, F.; Zhang, C.; Xiao, P.; Li, G. Biomedical Applications and Challenges of In-body Implantable Antenna for Implantable Medical Devices: A Review. *AEU-Int. J. Electron. Commun.* **2023**, *174*, 155053. [[CrossRef](#)]
- Niotaki, K.; Carvalho, N.B.; Georgiadis, A.; Gu, X.; Hemour, S.; Wu, K.; Matos, D.; Belo, D.; Pereira, R.; Figueiredo, R.; et al. RF energy harvesting and wireless power transfer for energy autonomous wireless devices and RFIDs. *IEEE J. Microw.* **2023**, *3*, 763–782. [[CrossRef](#)]
- Stankiewicz, J.M. Analysis of the Influence of the Skin Effect on the Efficiency and Power of the Receiver in the Periodic WPT System. *Energies* **2023**, *16*, 2009. [[CrossRef](#)]
- Li, M.; Khaleghi, A.; Hasanvand, A.; Narayanan, R.P.; Balasingham, I. A New Design and Analysis for Metasurface-Based Near-field Magnetic Wireless Power Transfer for Deep Implants. *IEEE Trans. Power Electron.* **2024**, *39*, 6442–6454. [[CrossRef](#)]

9. Shao, Y.; Kang, N.; Zhang, H.; Ma, R.; Liu, M.; Ma, C. A lightweight and robust drone MHz WPT system via novel coil design and impedance matching. *IEEE Trans. Ind. Appl.* **2023**, *59*, 3851–3864. [[CrossRef](#)]
10. Sun, G.; Muneer, B.; Li, Y.; Zhu, Q. Ultracompact implantable design with integrated wireless power transfer and RF transmission capabilities. *IEEE Trans. Biomed. Circuits Syst.* **2018**, *12*, 281–291. [[CrossRef](#)]
11. Aboulalaa, M.; Pokharel, R.K.; Kaho, T. Extended Embedded Depth Using Cascaded Resonators Near-field WPT System with High Efficiency for Biomedical Implants. In Proceedings of the 2023 IEEE/MTT-S International Microwave Symposium-IMS 2023, San Diego, CA, USA, 11–16 June 2023; pp. 887–890.
12. Verma, S.; Rano, D.; Hashmi, M. On the Use of Dual-Band SIMO and MIMO Based Defected Ground Structures in the Design, Characterization, and Validation of RF WPT System. *IEEE Trans. Instrum. Meas.* **2023**, *72*, 8003610. [[CrossRef](#)]
13. Jabbari, A.; Simovski, C.; Mollaei, M.S. Tunable Dual-Band High Impedance Coil for Wireless Power Transfer Applications. *IEEE Trans. Antennas Propag.* **2023**, *71*, 9467–9476. [[CrossRef](#)]
14. Zhang, Z.; Pang, H.; Georgiadis, A.; Cecati, C. Wireless power transfer—An overview. *IEEE Trans. Ind. Electron.* **2018**, *66*, 1044–1058. [[CrossRef](#)]
15. Bercich, R.A.; Duffy, D.R.; Irazoqui, P.P. Far-field RF powering of implantable devices: Safety considerations. *IEEE Trans. Biomed. Eng.* **2013**, *60*, 2107–2112. [[CrossRef](#)] [[PubMed](#)]
16. Sharma, D.; Kumar, S.; Singh, N.; Kanaujia, B.K.; Singh, S.P.; Lay-Ekuakille, A. Far-Field Wireless Power Transmission and Measurement for a Leadless Transcatheter Pacing System. *IEEE Trans. Instrum. Meas.* **2023**, *72*, 5503912. [[CrossRef](#)]
17. Park, J.H.; Tran, N.M.; Hwang, S.I.; Kim, D.I.; Choi, K.W. Design and implementation of 5.8 GHz RF wireless power transfer system. *IEEE Access* **2021**, *9*, 168520–168534. [[CrossRef](#)]
18. Yousaf, M.; Mabrouk, I.B.; Faisal, F.; Zada, M.; Bashir, Z.; Akram, A.; Nedil, M.; Yoo, H. Compacted conformal implantable antenna with multitasking capabilities for ingestible capsule endoscope. *IEEE Access* **2020**, *8*, 157617–157627. [[CrossRef](#)]
19. Zhou, J.; Zhang, P.; Han, J.; Li, L.; Huang, Y. Metamaterials and metasurfaces for wireless power transfer and energy harvesting. *Proc. IEEE* **2021**, *110*, 31–55. [[CrossRef](#)]
20. Haerinia, M.; Shadid, R. Wireless power transfer approaches for medical implants: A review. *Signals* **2020**, *1*, 209–229. [[CrossRef](#)]
21. Song, M.; Jayathurathnage, P.; Zanganeh, E.; Krasikova, M.; Smirnov, P.; Belov, P.; Kapitanova, P.; Simovski, C.; Tretyakov, S.; Krasnok, A. Wireless power transfer based on novel physical concepts. *Nat. Electron.* **2021**, *4*, 707–716. [[CrossRef](#)]
22. Zhang, Y.; Zhang, X.; He, D.; Tang, D.; Chen, Z. Design of a mid-field wireless power transmission system for deep-tissue implants. *Technol. Health Care* **2023**, *32*, 1341–1349. [[CrossRef](#)] [[PubMed](#)]
23. Joshi, A.C.; Dash, J.C.; Sarkar, D. Parasitic Patch-based Power Transfer Efficiency Enhancement of WPT Systems using Circularly Polarized Antennas for IMDs. *Authorea Preprints* **2023**. [[CrossRef](#)]
24. Das, R.; Yoo, H. A multiband antenna associating wireless monitoring and nonleaky wireless power transfer system for biomedical implants. *IEEE Trans. Microw. Theory Tech.* **2017**, *65*, 2485–2495. [[CrossRef](#)]
25. Basir, A.; Yoo, H. Efficient wireless power transfer system with a miniaturized quad-band implantable antenna for deep-body multitasking implants. *IEEE Trans. Microw. Theory Tech.* **2020**, *68*, 1943–1953. [[CrossRef](#)]
26. Iqbal, A.; Al-Hasan, M.; Mabrouk, I.B.; Basir, A.; Nedil, M.; Yoo, H. Biotelemetry and wireless powering of biomedical implants using a rectifier integrated self-diplexing implantable antenna. *IEEE Trans. Microw. Theory Tech.* **2021**, *69*, 3438–3451. [[CrossRef](#)]
27. Shaw, T.; Samanta, G.; Mitra, D. Efficient wireless power transfer system for implantable medical devices using circular polarized antennas. *IEEE Trans. Antennas Propag.* **2020**, *69*, 4109–4122. [[CrossRef](#)]
28. Shah, S.M.A.; Zada, M.; Nasir, J.; Owais, O.; Yoo, H. Electrically-small antenna with low SAR for scalp and deep tissue biomedical devices. *IEEE Access* **2022**, *10*, 90971–90981. [[CrossRef](#)]
29. Kiourti, A.; Nikita, K.S. A review of in-body biotelemetry devices: Implantables, ingestibles, and injectables. *IEEE Trans. Biomed. Eng.* **2017**, *64*, 1422–1430. [[CrossRef](#)] [[PubMed](#)]
30. Shah, S.A.A.; Yoo, H. Radiative near-field wireless power transfer to scalp-implantable biotelemetric device. *IEEE Trans. Microw. Theory Tech.* **2020**, *68*, 2944–2953. [[CrossRef](#)]
31. Yadav, M.P.; Singh, R.K.; Ray, K.P. A Comparative Investigation on Effect of Coupling in Aperture Coupled Microstrip Antennas. *Prog. Electromagn. Res. C* **2022**, *124*, 69–79. [[CrossRef](#)]
32. Hasgall, P.A.; Di Gennaro, F.; Baumgartner, C.; Neufeld, E.; Lloyd, B.; Gosselin, M.C.; Payne, D.; Klingenböck, A.; Kuster, N. *IT'IS Database for Thermal and Electromagnetic Parameters of Biological Tissues*; ScienceOpen, Inc.: Lexington, MA, USA, 2018; Version 4.0, 15.
33. Nguyen, N.; Ha-Van, N.; Seo, C. Midfield wireless power transfer for deep-tissue biomedical implants. *IEEE Antennas Wirel. Propag. Lett.* **2020**, *19*, 2270–2274. [[CrossRef](#)]
34. Iqbal, A.; Sura, P.R.; Al-Hasan, M.; Mabrouk, I.B.; Denidni, T.A. Wireless power transfer system for deep-implanted biomedical devices. *Sci. Rep.* **2022**, *12*, 13689. [[CrossRef](#)] [[PubMed](#)]

Disclaimer/Publisher's Note: The statements, opinions and data contained in all publications are solely those of the individual author(s) and contributor(s) and not of MDPI and/or the editor(s). MDPI and/or the editor(s) disclaim responsibility for any injury to people or property resulting from any ideas, methods, instructions or products referred to in the content.